DRAG REDUCTION OF RECTANGULAR RIBLETS IN A POSITIVE PRESSURE GRADIENTS DUCT FLOW

Entian LI[1], Xiang HU[1], Pei YAO[1]

Streamwise-aligned rectangular riblets are introduced to a positive pressing gradients pipe flow in this study. A detailed experimental system is discussed. Pressure drop is provided, and the drug reduction rate is analyzed. To explore the mechanism of drag reduction of riblets, a visualization test by PIV is conducted, and the flow field is presented and discussed. A discussion of the effects of the riblets on pressing pipe flow is given, and a hypothesis that the drag reduction of riblets is the competition results of the drag-reducing effect and the drag-increasing effect is proposed and discussed.

Keywords: Drag reduction, turbulence, flow field, flow visualization, riblets.

1. Introduction

Energy efficiency is considered to be the fifth largest energy source followed coal, oil, natural gas and electricity by some Chinese scientists [1]. Many countries take energy saving as the top aim in industrial and transportation industry. In transportation, a great proportion of energy is consumed to overcome resistance, resulting in a lot of energy consumption. Especially for long-distance fluid pipeline transportation, almost 100% of the energy supplied by pumps is used to overcome the resistance. Drag reduction has become the primary consideration for design of long-distance transportation pipeline. Application of drag reduction surface design will also bring great benefits to aeronautics, astronautics, navigation, and ground vehicles. Therefore, research on drag reduction saving in pipelines is of great significance.

The viewpoint that the frictional drag of the fluid flowing over a smooth surface is minimal has affected the researchers for a long time. Until the middle of 1960s, when Langley Research Center at National Aeronautics and Space Administration (NASA) found that the frictional drag of some specific microstructured surface was smaller than that of the smooth surface. Walsh [2-4] was committed to optimizing the shape and size of drag reduction riblets, hoping to get a maximum drag reduction rate at Langley Research Center. Their series of

[1] Changzhou University, China, e-mail: let@cczu.edu.cn

experiments came to a conclusion that triangular is the most effective microstructural shapes for drag reduction and up to 7%-8% percent occurred for triangular grooved riblets having s^+=15 and h^+=13. Bacher [5] obtained a maximum 25% drag reduction of triangular riblets surface by calculating measured by hot-film anemometry using boundary layer momentum integral method. By using the same method as Bacher [5], Gallagher [6] got 20% local skin friction reduction near the end of the riblets plate, but no drag reduction. Lazos [7] gained a maximum drag reduction of 8% which was equal to the symmetric V-groove by testing rectangular grooved surfaces with thin-element riblets in a low-speed wind tunnel. Rohr [8] found there were no significant differences in drag reduction of triangular riblets between internal and external flows by using an assortment of drag measuring techniques. Hot-wire anemometer was used by Park [9] to record the streamwise velocity field of the triangular riblets surface and a 4% drag reduction rate was obtained. Bechert [10] tested conventional ribbed surfaces with triangular and semi-circular grooves, and confirmed about 5% drag reduction. And then, modified thin-element riblets were also tested and a maximum drag reduction of 9.9% was obtained by Bechert [10]. By using direct numerical simulations method, El-Samni [11] got a greater drag reduction rate for modified thin-element riblets than Bechert [10]. Tsunoda [12] measured the instantaneous velocity fields of riblet surfaces by using a particle image velocimetry (PIV) and got a reduction ratio of the skin friction coefficient up to 8%. By using Large Eddy Simulation, Peet [13] yielded at least 50% increase of drag reduction rate by modifying the traditional straight triangular cross-section riblets to sinusoidal-like triangular cross-section riblets. Martin [14] modeled blade, sawtooth, and scalloped riblets with ANSYS Fluent 16.0 and proposed optimized riblts for commercial applications of blade riblets with an s^+=15-20 and height of h^+= 8-10. And also, by numerical simulating, Martin [15] compared the drag reduction effects of continuous riblet structures to segmented riblet structures and found that continuous configurations have an approximately 10% greater drag reduction than that of the aligned-segmented and staggered-segmented configurations.

Through flow visualization experiments, Bacher and Smith [1985] found that the cross-stream secondary vortices formed at the top of the riblets peaks can weaken the streamwise vortices above the riblets and remain the low-speed fluid within the valleys resulting in an inhibition of formation and spreading of the low-speed streaks. The “Secondary Vortices Theory” proposed by Bacher and

Smith [1985] was confirmed and enriched by later researchers. Choi [16-17] believed the interaction of riblets surface and the streamwise vortex inhibits further development of streamwise vortices transition delay and drag reduction. Walsh [18] considered that the low speed quieter fluid with low friction resistance is retained at the bottom of riblet valleys resulting in total resistance reducing, which was confirmed by Park [9]. Vukoslavcevic [19] attributed the reason for drag reduction to the friction resistance decreases much more at the bottom of the riblets than the friction resistance increases at the top of the riblets. Choi [20] believed that only a small part of riblets surface exposed in the high shear rate fluid induced by streamwise vortices, which result in viscous sub-layer thickness increasing and viscous drag decreasing. Huang [21] attributed the reason of the drag reduction effect of riblets to the competition results of “peak effect” and “restriction effect”. “Protrusion Height Theory” proposed by Bechert [22], confirmed and enriched by Suzuki [23], Lee [24], Jung, [25], Bixler [26] is another mechanism of drag reduction accepted by many researchers. According to Bechert [22], the so-called protrusion height refers to the distance from the apparent origin and riblets tips. In the riblets valleys below the apparent origin, the flow is viscous flow, which is equivalent to increasing the thickness of the viscous sublayer in the boundary layer and reducing the average velocity gradient near the wall. Therefore, the Protrusion Height Theory holds that when the fluid flows through the ribbed surface, the transient spanwise flow caused by turbulence is hindered, which reduces the turbulent kinetic energy in the entire boundary layer, thus reducing the friction resistance of the ribbed surface.

The bulk of the surveys have been conducted mainly on Zero Pressure Gradient external flow over a ribbed surface. But many practical implementations will expose riblets to pressing pipe flow for its great potential benefits in energy utilization. There were only a very small part of investigations have been done on internal flow over ribbed surfaces. Enyutin [27], Liu [28], Rohr [8] found that drag reduction rate of internal flow in round ribbed pipe was a little less than that of external flows. And a conclusion that riblets surfaces have no overall trend of drag reduction rate over smooth plate surface in rectangular duck flow was drawn by Dean [29], who suggested that additional studies should be performed using numerical simulation method or flow field display techniques.

The aim of this paper is to develop a flow field visualization experiment to find out the intrinsic links between characteristics distribution of flow parameters and the drag reduction of rectangular pressing pipe flow using Particle Image

Velocimetry (PIV) system. Moreover, the measurements of pressure drop both on ribbed surface and on smooth surface are collected and compared in this study. And the drag reduction performance in different scenarios are presented and discussed.

2. Experimental

A closed test loop consists of a test section, a water tank, a centrifugal pump, a differential pressure transmitter, an electromagnetic flowmeter, a retractor, a stabilizer, a diffuser, control valves and the other necessary elements. Fig.1 shows the structure of experimental system. The centrifugal pump recirculated water through the closed loops. The stabilizer was placed prior to the inlet of the rectangular pipe for keeping flow stable. The differential pressure transmitter (Shanghai Win-win Automation Equipment Co. Ltd., 0-3kPa measuring range and 1‰ measuring accuracy) was responsible for measuring pressure drop. The two pressure taps of the differential pressure transmitter were installed in the middle of the test section respectively, 2.8m from each other. The flow rate was measured using the electromagnetic flowmeter (Tianjin Guanghua Kaite Flow Instrument Co., Ltd, measuring accuracy of ±0.01 m3/h). The experiments were conducted using tap water of 25±0.5℃. The test section was an organic glass rectangular pipe, 7m in length, and cross-section of 60mm× 100mm. The length can guarantee turbulent flow in the pipe is a fully developed one. The inner wall of the test section was removable and could be fitted with ribbed surface plates or smooth surface plate by inserting them into the slot.

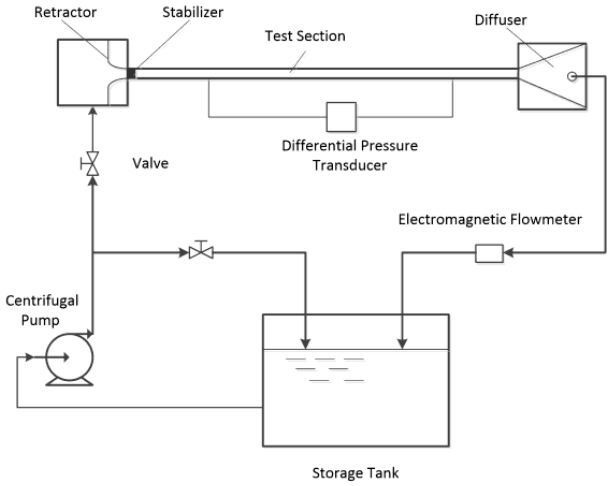

Fig. 1. Schematic of the experimental setup

The streamwise-aligned riblets used in present experiments have rectangular cross-section and were carved on the surface an organic glass plate by laser engraving machine such that the ridges of riblets were equal to the base surface, as shown in Fig. 2. The dimensions of riblet are defined by height (*h*), spacing (*s*), and width (*t*) shown in Table1. The uncarved blank plate surface was used as the smooth surface.

In present studies, the PIV measurement in *xy* plane is performed to compare the flow field over the ribbed surfaces with that over the smooth surface. The PIV measurement system used in the experiments consist of the imaging system (including a double-pulsed Nd:YAG laser, laser sheet optics and silicon dioxide tracking particles), the image acquisition system (including a charge-coupled device camera (CCD) and a synchronizer, and an image analysis) and the display system (including an image-processing software MicroVec V3 and a computer). The double-pulsed laser (KSP200) is the light source for producing the high energy (200 mJ) pulses of light green (532 nm) with frequency of 15 Hz during five nanoseconds. The proper-sized lightsheet thickness (0.5 to 1 mm) can be obtained by adjusting the spherical lens of the laser sheet optics. The Synchronizer controls the timing and sequencing of double-pulsed lasers, the CCD, and the computer works synergistically so as to take a clear PIV photograph with a resolution of 768×484 pixels. Furthermore, the hollow glass microspheres with an average grain diameter of 5μm and specific gravity of 1.05 were used as tracer particles. The optical configuration for PIV measurement arrangement in Cartesian coordinates is schematically shown in Fig. 3. The CCD is used to record the image of the particle in the flow with the image-acquiring rate of 30 frames per second. MicroVec V3 software was used to deal with the images obtained from the flow field.

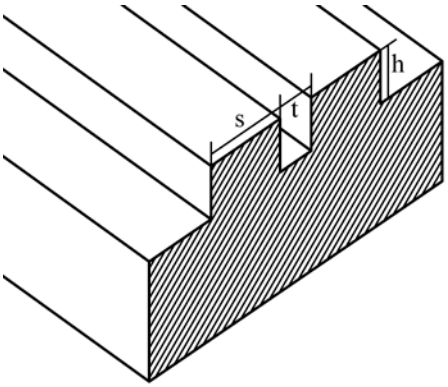

Fig. 2. Schematic diagram of the ribbed plate

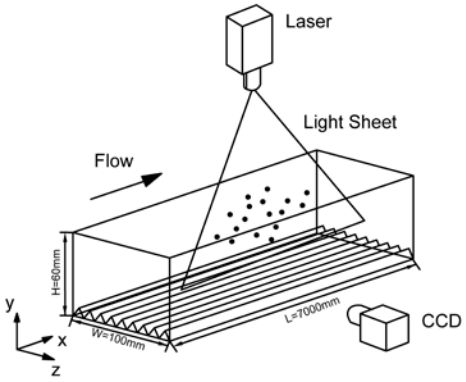

Fig. 3. Schematic of PIV arrangement

Table 1

Detailed parameter of riblets used in the experiment

Case	Spacing (*s*/mm)	Depth (*h*/mm)	Width (*t*/mm)
1	0.6	0.3	1
2	0.6	0.5	1
3	0.6	0.7	1
4	1	0.3	0.6
5	1	0.5	0.6
6	1	0.7	0.6

3. Results and discussion

3.1. Drag reduction rate

The drag reduction rate can be calculated by the following equation:

$$DR\% = \frac{f_s - f_r}{f_s}, \tag{1}$$

where f_s is the Fanning friction factor of the smooth surface, and f_r is the Fanning friction factor of ribbed surfaces.

The Fanning friction factor (f) can be defined as below:

$$f = \frac{2\tau_w}{\rho U_\infty{}^2} = \frac{\Delta pHW}{\rho U_\infty{}^2 (H+W)L}, \tag{2}$$

Where τ_w is the wall shear stress, ρ is the fluid density, U_∞ is the freestream velocity. Δp presents the pressure drops measured by the two pressure taps of the differential pressure transmitter, L is the distance of the two pressure taps, W is the width of the rectangular pipe, and H represents the height of the rectangular pipe.

The dimensions of the turbulent flow structures vary as the flow properties change. For the convenience of comparing researchers developed in different flow conditions, it is helpful to use non-dimensional length values to characterize flow properties.

The dimensionless height and spacing of the riblets in wall units, marked $^+$, are calculated by multiplying they dimensional length by u_τ / υ as below.

$$h^+ = \frac{su_\tau}{\upsilon} \tag{3}$$

$$s^+ = \frac{su_\tau}{\upsilon}, \tag{4}$$

Where u_τ is the wall friction velocity which can be calculated as eq. (5) according to Flack [30]

$$u_\tau = U_\infty \sqrt{C_f / 2}, \tag{5}$$

The results of the drag reduction rate (DR) of ribbed surfaces calculated by Fanning friction factor with Eq. (1) are presented respectively as plots vs. s^+ in Fig. 4 along with the results reported by Bechert [10]. It can be seen from the plots, the drag reduction rate increases with the increase of s^+ to a maximum at s^+=12~18, and then turns to decrease with the further increase of s^+, the drag reduction rate of riblets surface 4, 5 and 6 decreases to zero at s^+>20, s^+>25 for riblets surface 2 and 3, and s^+>33 for riblets surface 1. As s^+ continue to increase, the drag-reducing effect of riblets turns into drag-increasing effect. This trend was also discovered by Bechert [10], El-Samni [11], Martin [14].

It can also be concluded from Fig. 4, the s^+ rang corresponding to positive drag reduction rate of riblets surface 1 is the widest, and drag reduction effect of riblets surface 2 and 3 is optimal. The maximum drag reduction rate of this experiment is about 8% less than 9.9% reported by Bechert [10]. We believe the differences of experimental conditions contribute to the different results. Firstly, the rectangular pressing pipes used in the experiments are totally different in cross-sectional area, 60 mm × 100 mm in our experiments, and 250 mm × 850 mm in Bechert's experiments. Water was used in our experiments which is a lower viscosity fluid compared to oil used in Bechert's experiments. Secondly, the experiments were carried out with a zero pressure gradient in Bechert's experiments, while our experiment was performed on a pressing pipe with a positive pressure gradient. Thirdly, the riblets used in Bechert's experiments were blade riblets, the thickness of which is much thinner than that in our experiments.

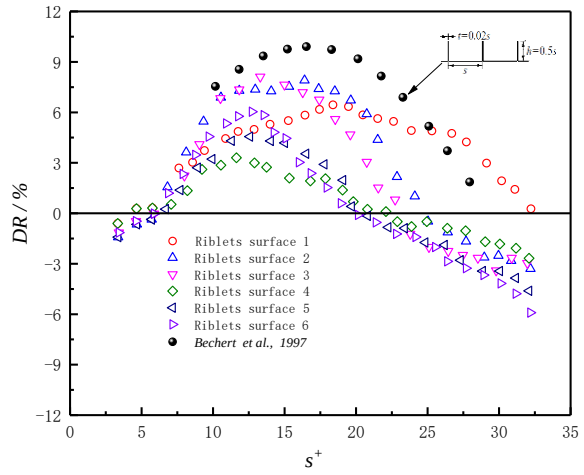

Fig. 4. Comparison of drag reduction rate between present results and Bechert [10]

3.2. Mean velocity

The dimensionless distance from the surfaces y^+ ($y^+ = yu_\tau / \upsilon$) was plotted on the horizontal *x*-axis against the dimensionless mean velocity u^+ ($u^+ = u / u_\tau$) on the vertical *y*-axis in Fig. 5.

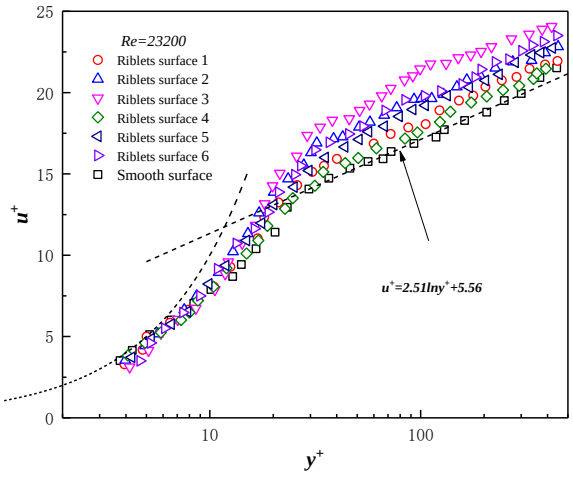

Fig. 5 Mean velocity profile at Re=23200

Fig. 5 shows the mean velocity profiles in the present experiment agree fairly well with the Law of the Wall profile of Newtonian fluid flow. As the profiles show there is no significant difference in mean velocity between ribbed

surfaces and smooth surface in viscous sub-layer ($0<y^+<5$) and buffer layer ($5<y^+<30$). But in logarithmic law layer which can be described as $u^+ = A\ln y^+ + B$, the mean velocity is shifted upwards by riblets with a steeper gradient resulting in the increase of value *A* and *B*, indicating that the boundary layer is thickened. This distinguishing feature can also be seen visually from the mean velocity distribution in Fig. 6. The experimental results of Wang [31] and the direct numerical simulation results of Choi [16] agree with this well. This distinguishing feature of boundary layer thickening of ribbed surfaces is resulting in near-wall mean velocity gradient decreasing comparing to that of the smooth surface, indicating a lower viscous shear stress caused by riblets near the wall. A similar conclusion was proposed by Bechert [32], Jung [25] and Bixler [26].

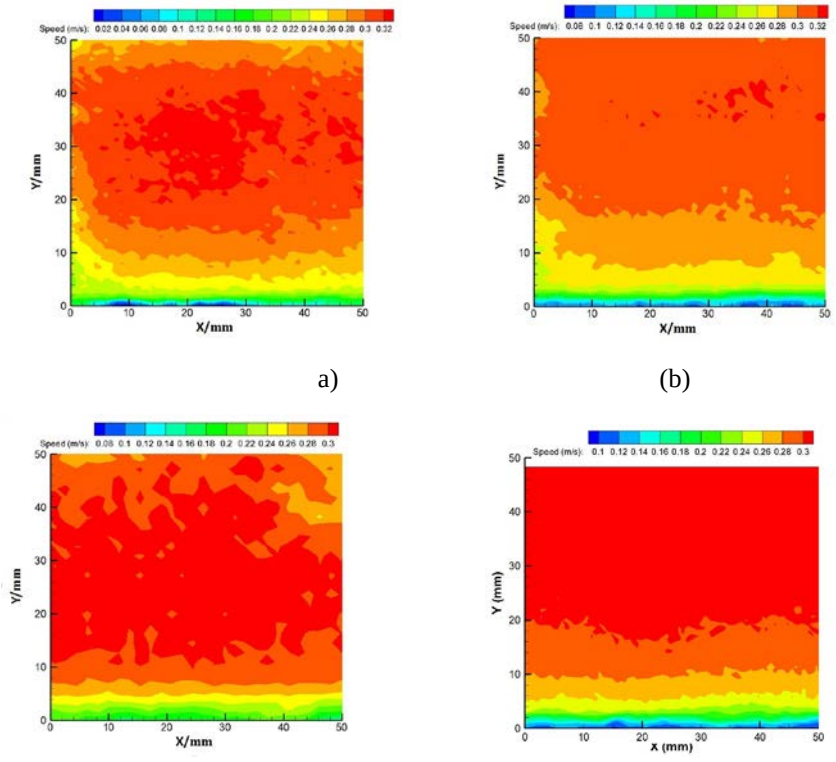

Fig. 6 Mean velocity distribution sampled at Re=23200; (a) Smooth surface (b) Riblets 1, (c) Riblets surface 2, and (d) Riblets surface 3.

3.3Reynolds shear stress

The distribution of the dimensionless Reynolds stress $-\overline{u'^{+}v'^{+}} = -\rho\overline{u'v'}/u_{\tau}^{2}$ at *Re*=23200 is shown in Fig. 7 shows. As can be seen from the plots, compared to smooth surface, Reynolds shear stress of ribbed surfaces is significantly inhibited. As a result, riblets weaken the components of fluctuating velocity and Reynolds stress. Thus, the momentum exchange between the high-speed fluid and low-speed fluid as well as the events of ejection and sweep are reduced. It can also be seen from Fig. 7 that the inhibition effect riblets surface 3 on the two fluctuation components is stronger than that of the other riblets surfaces.

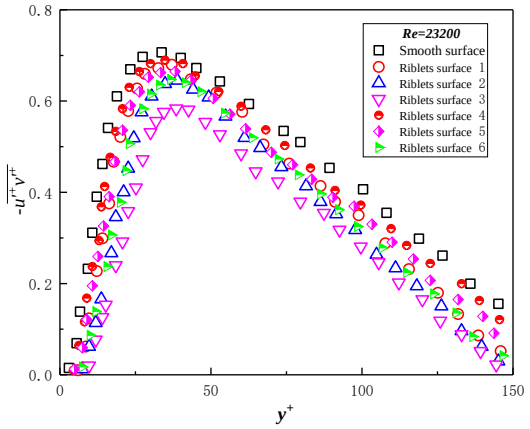

Fig. 7 Reynolds shear stress sampled at Re=23200

3.4 Turbulent intensities

Fig. 8 shows the distributions of streamwise and wall-normal turbulence intensities nondimensionalized by frictional velocity $u_{rms}^{+} = \sqrt{\overline{u'^{2}}}/u_{\tau}$ and $v_{rms}^{+} = \sqrt{\overline{v'^{2}}}/u_{\tau}$, where u' and v' represent the streamwise and wall-normal fluctuation velocity respectively. It can be concluded the trends of turbulence intensity of ribbed surfaces and smooth surface are same. Values of two turbulence intensities components u_{rms}^{+} and v_{rms}^{+} are very small in viscous sub-layer indicating turbulence is very weak but still exists and increase rapidly

with $y+$ increasing. After reaching the maximum, streamwise and wall-normal turbulence intensities are gradually weakened.

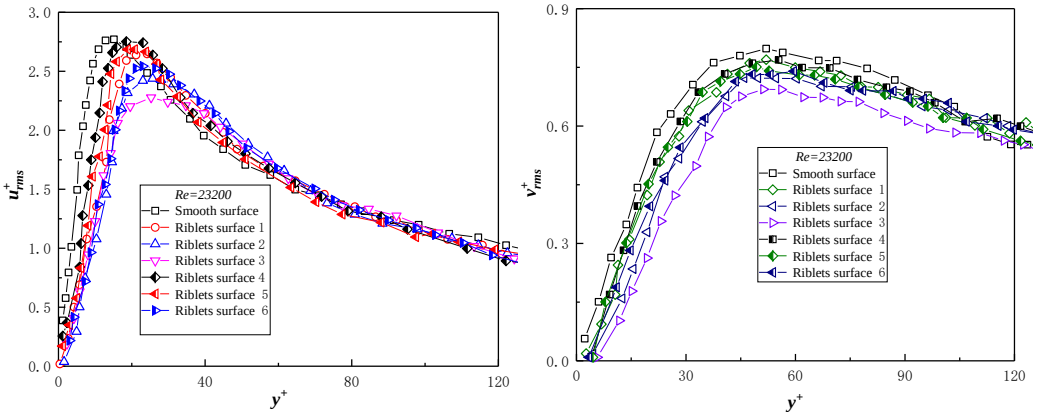

□ a□ □ b□

Fig. 8 Distribution of turbulent intensities at Re=23200: (a) streamwise (b) wall-normal.

According to fig.8 there is no significant difference in turbulence intensities between ribbed surfaces and smooth surface in viscous sub-layer. The u^+_{rms} of ribbed surfaces is smaller than that of smooth surface in buffer layer where is the main region that high-speed streaks and low-speed streaks exist, and the values v^+_{rms} of ribbed surfaces are obviously smaller than that of the smooth surface in buffer layer and logarithmic law layer, indicating an inhibition effect on turbulence intensities.

3.5. Mechanism analysis of drag-reduction

Riblets in laminar flow provide no benefit to drag reduction, and even impede the flow and cause drag-increasing. But in turbulence, riblets may work to drag reduction by the competition of drag-reducing effect and drag-increasing effect which are both caused by riblets and coexist. The schematic diagram of the competition of drag-increasing effect and drag-reducing effect by riblets is shown in Fig. 9.

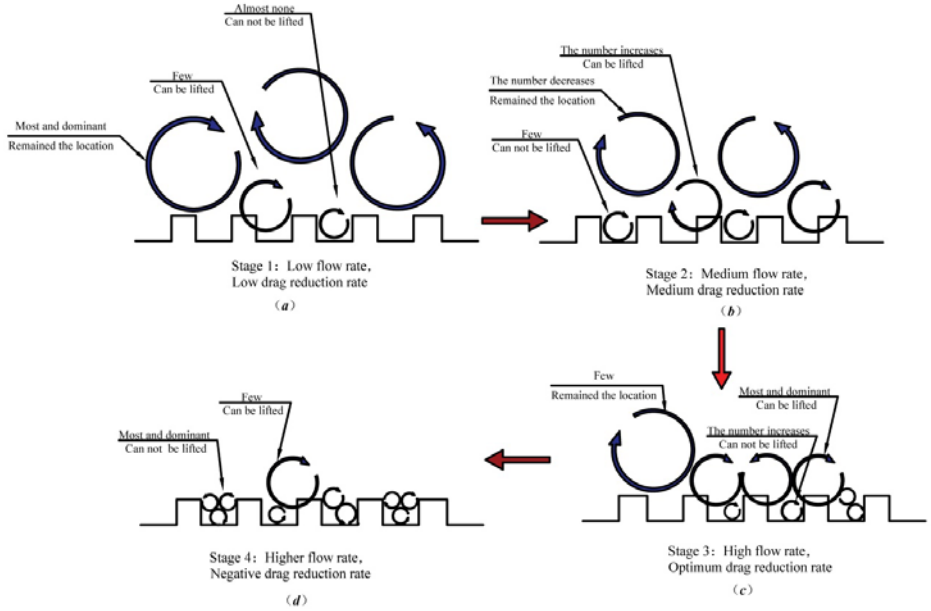

Fig. 9 Schematic diagram of the competition of drag-increasing effect and drag-reducing effect

Riblets can impede activities of the streamwise near-wall vortices by lifting vortices from the surface or by retaining the location of vortices which result in the weakening of the turbulence intensity, the decrease of the mean velocity and shear stress, the weakening of the momentum transfer and the two components of turbulent fluctuation, the reduction of the Reynolds shear stress and the widening of the low-speed streaks [10, 11, 15, 22, 26, 32, 33] indicating a drag-reducing effect. How well the vortices scale matches the spacing of riblets largely determines the drag-reducing effect of riblets [15]. Simultaneous riblets present drag-increasing effect by increasing the total wetted surface area and by interacting with the ejection and sweep motion of fluid which leads to a dramatic increase of shear stresses and turbulence intensity near the riblets tips [15, 20, 34]. The drag reduction effect of riblets depends on which of the two effects mentioned above occupies the dominant position. The drag reduction rate plot of riblets surface 3 in Fig. 4 is taken as an example to illuminate the mechanism of drag reduction.

As shown in Fig. 9, when the velocity of the fluid is low (s^+<10), drag-reducing effect occupies the dominant position, the drag-increasing effect is subordinate, and the increase of drag-increasing effect is slower than the drag-reducing effect. Whereas riblets show a fewer drag reduction rate due to the reason that in this case, the scale of the most of streamwise vortices

in the near wall region is much larger than the peak-to-peak spacing of the riblets, and only a very few vortices can be lifted by riblets as Fig. 9 (a) shown. As the velocity of the fluid increases ($10<\boldsymbol{s}^{+}<13$), the vortices scale decreases and matches the riblets spacing better and much more middle-scale vortices can be lifted by riblets as Fig. 9 (b) shown. As a result, the drag-reducing effect continues to be enhanced, and a greater drag reduction rate obtains due to the greater inhibition of the near-wall vortices activities. As decreases to the optimum with the increase of the fluid velocity ($\boldsymbol{s}^{+}\approx13$), vortices scale matches the riblets spacing best (shown in Fig. 9 (c)), resulting in the highest drag reduction rate due to the strongest inhibition of the near-wall vortices activities. Moreover, with the fluid velocity increasing ($\boldsymbol{s}^{+}>13$) drag-reducing effect still occupies the dominant position, but the growth of drag-reducing effect is slower than the drag-increasing effect causing the drag reduction rate of riblets declines regularly. The vortices scale further decreases and more small vortices crush into the valleys，exposing a larger wetted surface area of the valleys to the sweep motion of the fluids, which is translated into a drag-increasing effect by increasing shear stress the two components of turbulent fluctuation. The drag reduction rate decreases to zero at $s^{+}\approx23$ indicating drag-reducing effect and drag-increasing effect are counteracted each other. Then, the drag-increasing effect occupies the dominate position，the drag reduction rate becomes negative and decreases with further increasing of s^{+} as shown in Fig. 9 (d).

4. Conclusions

The drag reduction performance and detailed flow field structure of ribbed surfaces and smooth surface are investigated experimentally in this study to confirm the effects of streamwise-aligned rectangular riblets on a positive pressure gradients duct flow.

To inspect the flow behavior of surfaces with different surface microtextures, the pressure drop is measured. The maximum drag-reduction rate of 8% is obtained at $s^{+}=13$ for riblets surface 3.

To reveal the drag reduction mechanisms of microstructures, the PIV measurement technique was used to obtain the instantaneous mean velocity fields. It is confirmed from this paper riblets thickened the boundary layer, thus the near-wall mean velocity gradient is reduced, leading to a lower viscous shear stress. The Reynolds shearing stress of ribbed surfaces decreases in buffer layer and logarithmic law layer of the boundary layer, which is due to a decrease in the

contribution of the random component of the Reynolds shearing stress. The vorticity near the wall of ribbed surfaces decreases, due to the drag-reducing effect of the riblets tips by inhibiting the activities of the streamwise near-wall vortices.

In a summary, it can be a beneficial means to introduce streamwise-aligned riblets with the appropriate s^+ to an application in a long-distance pipeline.

Acknowledgments

This work was supported by National Natural Science Foundation of China (No. 51376026) and Jiangsu Overseas Visiting Scholar Program for University Prominent Yong & Middle-aged Teachers and Presidents.

R E F E R E N C E S

[1]. *F. C. Li*, Turbulent drag reduction by surfactant additives, Wiley, 2012., Hoboken, N.J., 2012.

[2]. *M. J. Walsh*, "Drag characteristics of V-groove and transverse curvature riblets", in Viscous Flow Drag Reduction, **VOL. 72**, 1980, pp. 168-184

[3]. *M.J. Walsh*, "Turbulent boundary layer drag reduction using riblets", in 20th Aerospace Sciences Meeting, American Institute of Aeronautics and Astronautics, 1982.

[4]. *M. J. Walsh, A. Lindemann*, "Optimization and application of riblets for turbulent drag reduction", in 22nd Aerospace Sciences Meeting, American Institute of Aeronautics and Astronautics, 1984.

[5]. *E. Bacher, C. Smith*, "A combined visualization-anemometry study of the turbulent drag reducing mechanisms of triangular micro-groove surface modifications", in Shear Flow Control Conference, American Institute of Aeronautics and Astronautics, Mar. 12-14, 1985.

[6]. *J. Gallagher, A. Thomas*, "Turbulent boundary layer characteristics over streamwise grooves", in American Institute of Aeronautics and Astronautics, Applied Aerodynamics Conference, Seattle, Wa, Aug. 21-23, 1984.

[7]. *B. Lazos, S. P. Wilkinson*, "Turbulent viscous drag reduction with thin-element riblets", in Aiaa Journal, **VOL. 26** (4), 1988, pp. 496-498

[8]. *J. J. Rohr, G. W. Andersen, L. W. Reidy, E. W. Hendricks*, "A comparison of the drag-reducing benefits of riblets in internal and external flows", in Experiments in Fluids, **VOL. 13** (6), 1992, pp. 361-368

[9]. *S. R. Park, J. M. Wallace*, "Flow alteration and drag reduction by riblets in a turbulent boundary layer", in Aiaa Journal, **VOL. 32** (1), 1994, pp. 31-38

[10]. *D. W. Bechert, M. Bruse, W. Hage, d. H. Van, J. G. T, G. Hoppe*, "Experiments on drag-reducing surfaces and their optimization with an adjustable geometry", in Journal of Fluid Mechanics, **VOL. 338** (338), 1997, pp. 59-87

[11]. *O. A. El-Samni, H. H. Chun, H. S. Yoon*, "Drag reduction of turbulent flow over thin rectangular riblets". in International Journal of Engineering Science, **VOL. 45** (2), 2007, pp. 436-454

[12]. *K. Tsunoda, N. Suzuki*, "Turbulence Characteristics in the Flowfield over a Heated Riblet Surface", in Transactions of the Japan Society of Mechanical Engineers, Part B, **VOL. 74(4)**, 2008, pp. 52-59

[13]. *Y. Peet, P. Sagaut, Y. Charron*, "Turbulent drag reduction using sinusoidal riblets with triangular cross-section", in 38th AIAA Fluid Dynamics Conference and Exhibit, 2008.

[14]. *S. Martin, B. Bhushan*, "Modeling and optimization of shark-inspired riblet geometries for low drag applications", in Journal of Colloid & Interface Science, **VOL. 474**, 2016, pp. 206-215

[15]. *S. Martin, B. Bhushan*, "Fluid flow analysis of continuous and segmented riblet structures", in Rsc Advances, **VOL. 6** (13), 2016, pp. 10962-10978

[16]. *K. S. Choi*, "Near-wall structure of a turbulent boundary layer with riblets", in Journal of Fluid Mechanics, **VOL. 208** (208), 1989, pp. 417-458

[17]. *K. S. Choi*, Effects of Longitudinal Pressure Gradients on Turbulent Drag Reduction with Riblets, Springer, Netherlands, 1990.

[18]. *M. J. Walsh*, "Viscous Drag Reduction in Boundary Layers", in Progress in Astronautics & Aeronautics, **VOL. 123**, 1990.

[19]. *P. Vukoslavcevic, J. M. Wallace, J. L. Balint*, "Viscous drag reduction using streamwise-aligned riblets", in Aiaa Journal, **VOL. 30** (4), 1992, pp. 1119-1122

[20]. *Choi, Haecheon, Moin, Parviz, Kim, John* "Direct numerical simulation of turbulent flow over riblets". in Journal of Fluid Mechanics, **VOL. 255** (-1), 1993, pp. 503-539

[21]. *C. Huang, D. Liu, J. Wei*, "Experimental study on drag reduction performance of surfactant flow in longitudinal grooved channels", in Chemical Engineering Science, **VOL. 152**, 2016, pp. 267-279

[22]. *D. W. Bechert, M. Bartenwerfer*, "The viscous flow on surfaces with longitudinal ribs", in Journal of Fluid Mechanics, **VOL. 206** (-1), 1989, pp. 105-129

[23]. *Y. Suzuki, N. Kasagi*, "Turbulent drag reduction mechanism above a riblet surface", in AIAA Journal, **VOL. 32** (9), 1994, pp. 1781-1790

[24]. *S.-J. Lee, S.-H. Lee*, "Flow field analysis of a turbulent boundary layer over a riblet surface", in Experiments in Fluids, **VOL. 30** (2), 2001, pp. 153-166

[25]. *Y. C. Jung, B. Bhushan*, "Biomimetic structures for fluid drag reduction in laminar and turbulent flows", in Journal of Physics Condensed Matter An Institute of Physics Journal, **VOL. 22** (3), 2010, pp. 035104

[26]. *G. D. Bixler, B. Bhushan*, "Fluid Drag Reduction with Shark‐Skin Riblet Inspired Microstructured Surfaces", in Advanced Functional Materials, **VOL. 23** (36), 2013, pp. 4507-4528

[27]. *G. V. Enyutin, Y. A. Lashkov, N. V. Samoilova*, "Drag reduction in riblet-lined pipes", in Fluid Dynamics, **VOL. 30** (1), 1995, pp. 45-48

[28]. *K. N. Liu, C. Christodoulou, O. Riccius, D. D. Joseph* "Drag reduction in pipes lined with riblets". in Aiaa Journal, **VOL. 28** (28), 1989, pp. 1697-1699

[29]. *B. Dean, B. Bhushan*, "The effect of riblets in rectangular duct flow", in Applied Surface Science, **VOL. 258** (8), 2012, pp. 3936-3947

[30]. *K. A. Flack, M. P. Schultz, J. M. Barros, Y. C. Kim*, "Skin-friction behavior in the transitionally-rough regime", in International Journal of Heat & Fluid Flow, **VOL. 61**, 2016, pp. 21-30

[31]. *J. J. Wang, S. L. Lan, G. Chen* "Experimental study on the turbulent boundary layer flow over riblets surface", in Fluid Dynamics Research, **VOL. 27** (4), 2000, pp. 217-229

[32]. *D. W. Bechert, M. Bartenwerfer, G. Hoppe, W. E. Reif*, "Drag reduction mechanisms derived from shark skin", in Icas, Congress, , London, England, September 7-12, 1986.

[33]. *J. H. Ng, R. K. Jaiman, T. T. Lim*, "Direct Numerical Simulation of Geometric Effects on Turbulent Flows over Riblets", in Aiaa Flow Control Conference, 2014.

[34]. *D. Y. Zhang, Y. H. Luo, L. I. Xiang, H. W. Chen*, "Numerical simulation and experimental study of drag-reducing surface of a real shark skin", in Journal of Hydrodynamics, SerB, **VOL. 23** (2), 2011, pp. 204-211.